

Study of $J/\psi \rightarrow \eta\phi\pi^+\pi^-$ at BESIII

M. Ablikim,¹ M. N. Achasov,^{8,a} X. C. Ai,¹ O. Albayrak,⁴ M. Albrecht,³ D. J. Ambrose,⁴³ A. Amoroso,^{47a,47c} F. F. An,¹ Q. An,⁴⁴ J. Z. Bai,¹ R. Baldini Ferroli,^{19a} Y. Ban,³⁰ D. W. Bennett,¹⁸ J. V. Bennett,⁴ M. Bertani,^{19a} D. Bettoni,^{20a} J. M. Bian,⁴² F. Bianchi,^{47a,47c} E. Boger,^{22,h} O. Bondarenko,²⁴ I. Boyko,²² R. A. Briere,⁴ H. Cai,⁴⁹ X. Cai,¹ O. Cakir,^{39a,b} A. Calcaterra,^{19a} G. F. Cao,¹ S. A. Cetin,^{39b} J. F. Chang,¹ G. Chelkov,^{22,c} G. Chen,¹ H. S. Chen,¹ H. Y. Chen,² J. C. Chen,¹ M. L. Chen,¹ S. J. Chen,²⁸ X. Chen,¹ X. R. Chen,²⁵ Y. B. Chen,¹ H. P. Cheng,¹⁶ X. K. Chu,³⁰ G. Cibinetto,^{20a} D. Cronin-Hennessy,⁴² H. L. Dai,¹ J. P. Dai,³³ A. Dbeysi,¹³ D. Dedovich,²² Z. Y. Deng,¹ A. Denig,²¹ I. Denysenko,²² M. Destefanis,^{47a,47c} F. De Mori,^{47a,47c} Y. Ding,²⁶ C. Dong,²⁹ J. Dong,¹ L. Y. Dong,¹ M. Y. Dong,¹ S. X. Du,⁵¹ P. F. Duan,¹ J. Z. Fan,³⁸ J. Fang,¹ S. S. Fang,¹ X. Fang,⁴⁴ Y. Fang,¹ L. Fava,^{47b,47c} F. Feldbauer,²¹ G. Felici,^{19a} C. Q. Feng,⁴⁴ E. Fioravanti,^{20a} M. Fritsch,^{15,21} C. D. Fu,¹ Q. Gao,¹ Y. Gao,³⁸ I. Garzia,^{20a} K. Goetzen,⁹ W. X. Gong,¹ W. Gradl,²¹ M. Greco,^{47a,47c} M. H. Gu,¹ Y. T. Gu,¹¹ Y. H. Guan,¹ A. Q. Guo,¹ L. B. Guo,²⁷ T. Guo,²⁷ Y. Guo,¹ Y. P. Guo,²¹ Z. Haddadi,²⁴ A. Hafner,²¹ S. Han,⁴⁹ Y. L. Han,¹ F. A. Harris,⁴¹ K. L. He,¹ Z. Y. He,²⁹ T. Held,³ Y. K. Heng,¹ Z. L. Hou,¹ C. Hu,²⁷ H. M. Hu,¹ J. F. Hu,^{47a} T. Hu,¹ Y. Hu,¹ G. M. Huang,⁵ G. S. Huang,⁴⁴ H. P. Huang,⁴⁹ J. S. Huang,¹⁴ X. T. Huang,³² Y. Huang,²⁸ T. Hussain,⁴⁶ Q. Ji,¹ Q. P. Ji,²⁹ X. B. Ji,¹ X. L. Ji,¹ L. L. Jiang,¹ L. W. Jiang,⁴⁹ X. S. Jiang,¹ J. B. Jiao,³² Z. Jiao,¹⁶ D. P. Jin,¹ S. Jin,¹ T. Johansson,⁴⁸ A. Julin,⁴² N. Kalantar-Nayestanaki,²⁴ X. L. Kang,¹ X. S. Kang,²⁹ M. Kavatsyuk,²⁴ B. C. Ke,⁴ R. Kliemt,¹³ B. Kloss,²¹ O. B. Kolcu,^{39b,d} B. Kopf,³ M. Kornicer,⁴¹ W. Kuehn,²³ A. Kupsc,⁴⁸ W. Lai,¹ J. S. Lange,²³ M. Lara,¹⁸ P. Larin,¹³ C. H. Li,¹ Cheng Li,⁴⁴ D. M. Li,⁵¹ F. Li,¹ G. Li,¹ H. B. Li,¹ J. C. Li,¹ Jin Li,³¹ K. Li,¹² K. Li,³² P. R. Li,⁴⁰ T. Li,³² W. D. Li,¹ W. G. Li,¹ X. L. Li,³² X. M. Li,¹¹ X. N. Li,¹ X. Q. Li,²⁹ Z. B. Li,³⁷ H. Liang,⁴⁴ Y. F. Liang,³⁵ Y. T. Liang,²³ G. R. Liao,¹⁰ D. X. Lin,¹³ B. J. Liu,¹ C. L. Liu,⁴ C. X. Liu,¹ F. H. Liu,³⁴ Fang Liu,¹ Feng Liu,⁵ H. B. Liu,¹¹ H. H. Liu,¹ H. H. Liu,¹⁵ H. M. Liu,¹ J. Liu,¹ J. P. Liu,⁴⁹ J. Y. Liu,¹ K. Liu,³⁸ K. Y. Liu,²⁶ L. D. Liu,³⁰ P. L. Liu,¹ Q. Liu,⁴⁰ S. B. Liu,⁴⁴ X. Liu,²⁵ X. X. Liu,⁴⁰ Y. B. Liu,²⁹ Z. A. Liu,¹ Zhiqiang Liu,¹ Zhiqing Liu,²¹ H. Loehner,²⁴ X. C. Lou,^{1,e} H. J. Lu,¹⁶ J. G. Lu,¹ R. Q. Lu,¹⁷ Y. Lu,¹ Y. P. Lu,¹ C. L. Luo,²⁷ M. X. Luo,⁵⁰ T. Luo,⁴¹ X. L. Luo,¹ M. Lv,¹ X. R. Lyu,⁴⁰ F. C. Ma,²⁶ H. L. Ma,¹ L. L. Ma,³² Q. M. Ma,¹ S. Ma,¹ T. Ma,¹ X. N. Ma,²⁹ X. Y. Ma,¹ F. E. Maas,¹³ M. Maggiora,^{47a,47c} Q. A. Malik,⁴⁶ Y. J. Mao,³⁰ Z. P. Mao,¹ S. Marcello,^{47a,47c} J. G. Messchendorp,²⁴ J. Min,¹ T. J. Min,¹ R. E. Mitchell,¹⁸ X. H. Mo,¹ Y. J. Mo,⁵ C. Morales Morales,¹³ K. Moriya,¹⁸ N. Yu. Muchnoi,^{8,a} H. Muramatsu,⁴² Y. Nefedov,²² F. Nerling,¹³ I. B. Nikolaev,^{8,a} Z. Ning,¹ S. Nisar,⁷ S. L. Niu,¹ X. Y. Niu,¹ S. L. Olsen,³¹ Q. Ouyang,¹ S. Pacetti,^{19b} P. Patteri,^{19a} M. Pelizzaeus,³ H. P. Peng,⁴⁴ K. Peters,⁹ J. L. Ping,²⁷ R. G. Ping,¹ R. Poling,⁴² Y. N. Pu,¹⁷ M. Qi,²⁸ S. Qian,¹ C. F. Qiao,⁴⁰ L. Q. Qin,³² N. Qin,⁴⁹ X. S. Qin,¹ Y. Qin,³⁰ Z. H. Qin,¹ J. F. Qiu,¹ K. H. Rashid,⁴⁶ C. F. Redmer,²¹ H. L. Ren,¹⁷ M. Ripka,²¹ G. Rong,¹ X. D. Ruan,¹¹ V. Santoro,^{20a} A. Sarantsev,^{22,f} M. Savrié,^{20b} K. Schoenning,⁴⁸ S. Schumann,²¹ W. Shan,³⁰ M. Shao,⁴⁴ C. P. Shen,² P. X. Shen,²⁹ X. Y. Shen,¹ H. Y. Sheng,¹ M. R. Shepherd,¹⁸ W. M. Song,¹ X. Y. Song,¹ S. Sosio,^{47a,47c} S. Spataro,^{47a,47c} B. Spruck,²³ G. X. Sun,¹ J. F. Sun,¹⁴ S. S. Sun,¹ Y. J. Sun,⁴⁴ Y. Z. Sun,¹ Z. J. Sun,¹ Z. T. Sun,¹⁸ C. J. Tang,³⁵ X. Tang,¹ I. Tapan,^{39c} E. H. Thorndike,⁴³ M. Tiemens,²⁴ D. Toth,⁴² M. Ullrich,²³ I. Uman,^{39b} G. S. Varner,⁴¹ B. Wang,²⁹ B. L. Wang,⁴⁰ D. Wang,³⁰ D. Y. Wang,³⁰ K. Wang,¹ L. L. Wang,¹ L. S. Wang,¹ M. Wang,³² P. Wang,¹ P. L. Wang,¹ Q. J. Wang,¹ S. G. Wang,³⁰ W. Wang,¹ X. F. Wang,³⁸ Y. D. Wang,^{19a} Y. F. Wang,¹ Y. Q. Wang,²¹ Z. Wang,¹ Z. G. Wang,¹ Z. H. Wang,⁴⁴ Z. Y. Wang,¹ T. Weber,²¹ D. H. Wei,¹⁰ J. B. Wei,³⁰ P. Weidenkaff,²¹ S. P. Wen,¹ U. Wiedner,³ M. Wolke,⁴⁸ L. H. Wu,¹ Z. Wu,¹ L. G. Xia,³⁸ Y. Xia,¹⁷ D. Xiao,¹ Z. J. Xiao,²⁷ Y. G. Xie,¹ G. F. Xu,¹ L. Xu,¹ Q. J. Xu,¹² Q. N. Xu,⁴⁰ X. P. Xu,³⁶ L. Yan,⁴⁴ W. B. Yan,⁴⁴ W. C. Yan,⁴⁴ Y. H. Yan,¹⁷ H. X. Yang,¹ L. Yang,⁴⁹ Y. Yang,⁵ Y. X. Yang,¹⁰ H. Ye,¹ M. Ye,¹ M. H. Ye,⁶ J. H. Yin,¹ B. X. Yu,¹ C. X. Yu,²⁹ H. W. Yu,³⁰ J. S. Yu,²⁵ C. Z. Yuan,¹ W. L. Yuan,²⁸ Y. Yuan,¹ A. Yuncu,^{39b,g} A. A. Zafar,⁴⁶ A. Zallo,^{19a} Y. Zeng,¹⁷ B. X. Zhang,¹ B. Y. Zhang,¹ C. Zhang,²⁸ C. C. Zhang,¹ D. H. Zhang,¹ H. H. Zhang,³⁷ H. Y. Zhang,¹ J. J. Zhang,¹ J. L. Zhang,¹ J. Q. Zhang,¹ J. W. Zhang,¹ J. Y. Zhang,¹ J. Z. Zhang,¹ K. Zhang,¹ L. Zhang,¹ S. H. Zhang,¹ X. J. Zhang,¹ X. Y. Zhang,³² Y. Zhang,¹ Y. H. Zhang,¹ Z. H. Zhang,⁵ Z. P. Zhang,⁴⁴ Z. Y. Zhang,⁴⁹ G. Zhao,¹ J. W. Zhao,¹ J. Y. Zhao,¹ J. Z. Zhao,¹ Lei Zhao,⁴⁴ Ling Zhao,¹ M. G. Zhao,²⁹ Q. Zhao,¹ Q. W. Zhao,¹ S. J. Zhao,⁵¹ T. C. Zhao,¹ Y. B. Zhao,¹ Z. G. Zhao,⁴⁴ A. Zhemchugov,^{22,h} B. Zheng,⁴⁵ J. P. Zheng,¹ W. J. Zheng,³² Y. H. Zheng,⁴⁰ B. Zhong,²⁷ L. Zhou,¹ Li Zhou,²⁹ X. Zhou,⁴⁹ X. K. Zhou,⁴⁴ X. R. Zhou,⁴⁴ X. Y. Zhou,¹ K. Zhu,¹ K. J. Zhu,¹ S. Zhu,¹ X. L. Zhu,³⁸ Y. C. Zhu,⁴⁴ Y. S. Zhu,¹ Z. A. Zhu,¹ J. Zhuang,¹ B. S. Zou,¹ and J. H. Zou¹

(BESIII Collaboration)

¹*Institute of High Energy Physics, Beijing 100049, People's Republic of China*²*Beihang University, Beijing 100191, People's Republic of China*³*Bochum Ruhr University, D-44780 Bochum, Germany*⁴*Carnegie Mellon University, Pittsburgh, Pennsylvania 15213, USA*⁵*Central China Normal University, Wuhan 430079, People's Republic of China*⁶*China Center of Advanced Science and Technology, Beijing 100190, People's Republic of China*⁷*COMSATS Institute of Information Technology, Lahore, Defence Road,**Off Raiwind Road, 54000 Lahore, Pakistan*

- ⁸*G. I. Budker Institute of Nuclear Physics SB RAS (BINP), Novosibirsk 630090, Russia*
⁹*GSI Helmholtzcentre for Heavy Ion Research GmbH, D-64291 Darmstadt, Germany*
¹⁰*Guangxi Normal University, Guilin 541004, People's Republic of China*
¹¹*GuangXi University, Nanning 530004, People's Republic of China*
¹²*Hangzhou Normal University, Hangzhou 310036, People's Republic of China*
¹³*Helmholtz Institute Mainz, Johann-Joachim-Becher-Weg 45, D-55099 Mainz, Germany*
¹⁴*Henan Normal University, Xinxiang 453007, People's Republic of China*
¹⁵*Henan University of Science and Technology, Luoyang 471003, People's Republic of China*
¹⁶*Huangshan College, Huangshan 245000, People's Republic of China*
¹⁷*Hunan University, Changsha 410082, People's Republic of China*
¹⁸*Indiana University, Bloomington, Indiana 47405, USA*
^{19a}*INFN Laboratori Nazionali di Frascati, I-00044 Frascati, Italy*
^{19b}*INFN and University of Perugia, I-06100 Perugia, Italy*
^{20a}*INFN Sezione di Ferrara, I-44122 Ferrara, Italy*
^{20b}*University of Ferrara, I-44122 Ferrara, Italy*
²¹*Johannes Gutenberg University of Mainz, Johann-Joachim-Becher-Weg 45, D-55099 Mainz, Germany*
²²*Joint Institute for Nuclear Research, 141980 Dubna, Moscow Region, Russia*
²³*Justus Liebig University Giessen, II. Physikalisches Institut, Heinrich-Buff-Ring 16, D-35392 Giessen, Germany*
²⁴*KVI-CART, University of Groningen, NL-9747 AA Groningen, The Netherlands*
²⁵*Lanzhou University, Lanzhou 730000, People's Republic of China*
²⁶*Liaoning University, Shenyang 110036, People's Republic of China*
²⁷*Nanjing Normal University, Nanjing 210023, People's Republic of China*
²⁸*Nanjing University, Nanjing 210093, People's Republic of China*
²⁹*Nankai University, Tianjin 300071, People's Republic of China*
³⁰*Peking University, Beijing 100871, People's Republic of China*
³¹*Seoul National University, Seoul 151-747, Korea*
³²*Shandong University, Jinan 250100, People's Republic of China*
³³*Shanghai Jiao Tong University, Shanghai 200240, People's Republic of China*
³⁴*Shanxi University, Taiyuan 030006, People's Republic of China*
³⁵*Sichuan University, Chengdu 610064, People's Republic of China*
³⁶*Soochow University, Suzhou 215006, People's Republic of China*
³⁷*Sun Yat-Sen University, Guangzhou 510275, People's Republic of China*
³⁸*Tsinghua University, Beijing 100084, People's Republic of China*
^{39a}*Istanbul Aydin University, Sefakoy, 34295 Istanbul, Turkey*
^{39b}*Dogus University, 34722 Istanbul, Turkey*
^{39c}*Uludag University, 16059 Bursa, Turkey*
⁴⁰*University of Chinese Academy of Sciences, Beijing 100049, People's Republic of China*
⁴¹*University of Hawaii, Honolulu, Hawaii 96822, USA*
⁴²*University of Minnesota, Minneapolis, Minnesota 55455, USA*
⁴³*University of Rochester, Rochester, New York 14627, USA*
⁴⁴*University of Science and Technology of China, Hefei 230026, People's Republic of China*
⁴⁵*University of South China, Hengyang 421001, People's Republic of China*
⁴⁶*University of the Punjab, Lahore 54590, Pakistan*
^{47a}*University of Turin, I-10125 Turin, Italy*
^{47b}*University of Eastern Piedmont, I-15121 Alessandria, Italy*
^{47c}*INFN, I-10125 Turin, Italy*
⁴⁸*Uppsala University, Box 516, SE-75120 Uppsala, Sweden*
⁴⁹*Wuhan University, Wuhan 430072, People's Republic of China*
⁵⁰*Zhejiang University, Hangzhou 310027, People's Republic of China*
⁵¹*Zhengzhou University, Zhengzhou 450001, People's Republic of China*
(Received 17 December 2014; published 20 March 2015)

Based on a sample of $2.25 \times 10^8 J/\psi$ events taken with the BESIII detector at the BEPCII collider, we present the results of a study of the decay $J/\psi \rightarrow \eta\phi\pi^+\pi^-$. The $Y(2175)$ resonance is observed in the

^aAlso at the Novosibirsk State University, Novosibirsk 630090, Russia.

^bAlso at Ankara University, 06100 Tandogan, Ankara, Turkey.

^cAlso at the Moscow Institute of Physics and Technology, Moscow 141700, Russia and the Functional Electronics Laboratory, Tomsk State University, Tomsk 634050, Russia.

invariant mass spectrum of $\phi f_0(980)$ with a statistical significance of greater than 10σ . The corresponding mass and width are determined to be $M = 2200 \pm 6(\text{stat}) \pm 5(\text{syst}) \text{ MeV}/c^2$ and $\Gamma = 104 \pm 15(\text{stat}) \pm 15(\text{syst}) \text{ MeV}$, respectively, and the product branching fraction is measured to be $\mathcal{B}(J/\psi \rightarrow \eta Y(2175), Y(2175) \rightarrow \phi f_0(980), f_0(980) \rightarrow \pi^+\pi^-) = (1.20 \pm 0.14(\text{stat}) \pm 0.37(\text{syst})) \times 10^{-4}$. The results are consistent within errors with those of previous experiments. We also measure the branching fraction of $J/\psi \rightarrow \phi f_1(1285)$ with $f_1(1285) \rightarrow \eta\pi^+\pi^-$ and set upper limits on the branching fractions for $J/\psi \rightarrow \phi\eta(1405)/\phi X(1835)/\phi X(1870)$ with $\eta(1405)/X(1835)/X(1870) \rightarrow \eta\pi^+\pi^-$ at the 90% confidence level.

DOI: 10.1103/PhysRevD.91.052017

PACS numbers: 12.39.Mk, 13.25.Gv, 14.40.Be, 14.40.Rt

I. INTRODUCTION

The $Y(2175)$, also referred to as the $\phi(2170)$ by the Particle Data Group (PDG 2014) [1], was first observed by the *BABAR* experiment [2] in the $e^+e^- \rightarrow \gamma_{\text{ISR}}\phi f_0(980)$ initial-state-radiation (ISR) process. It was later confirmed by the BESII experiment in $J/\psi \rightarrow \eta\phi f_0(980)$ decays [3] and via the same ISR process by the BELLE [4] and *BABAR* experiments [5] with increased statistics. Since the $Y(2175)$ resonance is produced via ISR in e^+e^- collisions, it is known to have $J^{PC} = 1^{--}$. This observation stimulated the speculation that the $Y(2175)$ may be an s -quark counterpart to the $Y(4260)$ [6,7], since both are produced in e^+e^- annihilation and exhibit similar decay patterns. Like for the $Y(4260)$, a number of different interpretations have been proposed for the $Y(2175)$ with predicted masses that are consistent, within errors, with the experimental measurements. These include an $s\bar{s}$ -gluon hybrid [8]; an excited ϕ state [9]; a tetraquark state [10]; a $\Lambda\bar{\Lambda}$ bound state [11,12]; and an ordinary $\phi f_0(980)$ resonance produced by interactions between the final state particles [13].

A recent review [14] discusses the basic problem of the large expected decay widths into two mesons, which contradicts experimental observations. Around the mass of the $Y(2175)$, there are two conventional $1^{--} s\bar{s}$ states in the quark model, 2^3D_1 and 3^3S_1 . According to Ref. [15], the width of the $3^3S_1 s\bar{s}$ state is expected to be about 380 MeV. The total width of the 2^3D_1 state from both 3P_0 and the flux tube model is expected to be around (150 ~ 250) MeV [9]. However, the predictions from these strong decay models sometimes deviate from the experimentally found width by a factor of 2 or 3. For comparison, the widths of the 3^3S_1 and 2^3D_1 charmonium are less than 110 MeV [16]. Fortunately, the characteristic decay modes of $Y(2175)$ as either a hybrid or $s\bar{s}$ state are quite different, which may

be used to distinguish the hybrid and $s\bar{s}$ schemes. The possibility of $Y(2175)$ arising from S -wave threshold effects is not excluded. As of now, none of these interpretations have been either established or ruled out by experiment. The confirmation and study of the $Y(2175)$ in $J/\psi \rightarrow \eta\phi\pi^+\pi^-$ with a large data sample is necessary for clarifying its nature.

The $J/\psi \rightarrow \eta\phi\pi^+\pi^-$ decay also offers a unique opportunity to investigate the properties of the $f_1(1285)$, the $\eta(1295)$, and the $\eta(1405)/\eta(1475)$ resonances. The $f_1(1285)$ is usually considered to be a member of the axial vector meson nonet, but the interpretation of the $\eta(1295)$ is less clear. Both the $f_1(1285)$ and the $\eta(1295)$ were seen in fixed target experiments, but the $\eta(1295)$ was not evident in central production, in $\gamma\gamma$ collisions, or in J/ψ decays. Therefore it has been speculated that either the $f_1(1285)$, at least in some cases, contains an $\eta(1295)$ component [17] or that the $\eta(1295)$ does not exist. The $\eta(1405)/\eta(1475)$ pseudoscalar was once regarded as a glueball candidate since it is copiously produced in J/ψ radiative decays [18] and there was only an upper limit from $\gamma\gamma$ collisions [19]. But this viewpoint changed when the $\eta(1405)/\eta(1475)$ was also observed in untagged $\gamma\gamma$ collisions [20] and in J/ψ hadronic decays.

In addition, two interesting resonances, the $X(1835)$ and the $X(1870)$, were observed in $J/\psi \rightarrow \gamma\pi^+\pi^-\eta'$ [21,22] and $J/\psi \rightarrow \omega\pi^+\pi^-\eta$ [23], respectively. The $X(1835)$, in particular, inspired many possible theoretical interpretations, including a $p\bar{p}$ bound state [24,25], a glueball [26–28], and final state interactions between a proton and an antiproton [29–31]. To better understand the properties of these two resonances, one needs to further study their production in different J/ψ decay modes. For example, the search for them in the $\eta\pi^+\pi^-$ mass spectrum recoiling against the ϕ in J/ψ decays would be rather interesting for clarifying their nature.

In this paper, we present a study of the decay $J/\psi \rightarrow \eta\phi\pi^+\pi^-$ with $\eta \rightarrow \gamma\gamma$ and $\phi \rightarrow K^+K^-$ decay modes using a sample of 2.25×10^8 J/ψ events collected with the Beijing Spectrometer (BESIII) located at the Beijing Electron-Positron Collider (BEPCII) [32]. The mass and width of the $Y(2175)$, as well as its production rate, are measured. In addition, the production rates of the $f_1(1285)$, the

^dPresent address: Istanbul Arel University, Kucukcekmece, Istanbul, Turkey.

^eAlso at University of Texas at Dallas, Richardson, Texas 75083, USA.

^fAlso at the PNPI, Gatchina 188300, Russia.

^gAlso at Bogazici University, 34342 Istanbul, Turkey.

^hAlso at the Moscow Institute of Physics and Technology, Moscow 141700, Russia.

$\eta(1405)/\eta(1475)$, the $X(1835)$, and the $X(1870)$ in J/ψ hadronic decays associated with a ϕ meson are investigated.

II. DETECTOR AND MONTE CARLO SIMULATION

The BESIII detector is a magnetic spectrometer [32] located at BEPCII, which is a double-ring e^+e^- collider with a design peak luminosity of $10^{33} \text{ cm}^{-2} \text{ s}^{-1}$ at a center-of-mass energy of 3.773 GeV. The cylindrical core of the BESIII detector consists of a helium-based main drift chamber (MDC), a plastic scintillator time-of-flight system (TOF), and a CsI (TI) electromagnetic calorimeter (EMC), which are all enclosed in a superconducting solenoidal magnet providing a 1.0 T magnetic field. The solenoid is supported by an octagonal flux-return yoke with modules of resistive plate muon counters interleaved with steel. The acceptance for charged particles and photons is 93% of the full 4π solid angle. The momentum resolution for a charged particle at 1 GeV/c is 0.5%, and the ionization energy loss per unit path-length (dE/dx) resolution is 6%. The EMC measures photon energies with a resolution of 2.5% (5%) at 1 GeV in the barrel (end caps). The time resolution for the TOF is 80 ps in the barrel and 110 ps in the end caps.

The GEANT-based simulation software BOOST [33] is used to simulate the desired Monte Carlo (MC) samples. An inclusive J/ψ MC sample is used to estimate the backgrounds. The production of the J/ψ resonance is simulated by the MC event generator KKMC [34,35], while the decays are generated by BesEvtGen [36–38] for known decay modes with branching fractions set at the PDG [1] world average values, and by the Lund-Charm model [39] for the remaining unknown decays.

In this analysis, a signal MC sample for the process $J/\psi \rightarrow \eta Y(2175)$, $Y(2175) \rightarrow \phi f_0(980)$ and $f_0(980) \rightarrow \pi^+\pi^-$, is generated to optimize the selection criteria and determine the detection efficiency. Since the J^{PC} of the $Y(2175)$ is 1^{--} , a P -wave orbital angular momentum is used for the η - $Y(2175)$ system, while S -wave is used for

the $\phi - f_0(980)$ and $\pi^+\pi^-$ systems. The shape of the $f_0(980)$ is parametrized with the Flatté formula [40], and the corresponding parameters are taken from the measurement of BESII [41]. For the signal MC sample of $J/\psi \rightarrow \phi\eta(1405)/f_1(1285)$, the angular distributions are also considered in the simulation.

III. EVENT SELECTION

To select candidate events of the process $J/\psi \rightarrow \eta\phi\pi^+\pi^-$ with $\phi \rightarrow K^+K^-$ and $\eta \rightarrow \gamma\gamma$, the following criteria are imposed on the data and MC samples.

We select charged tracks in the MDC within the polar angle range $|\cos\theta| < 0.93$ and require that the points of closest approach to the beam line be within ± 20 cm of the interaction point in the beam direction and within 2 cm in the plane perpendicular to the beam. The TOF and dE/dx information are combined to form particle identification (PID) confidence levels for the π , K , p hypotheses, and each track is assigned to the particle type corresponding to the hypothesis with the highest confidence level. Two kaon and two pion particles with opposite charges are required.

Photon candidates are reconstructed by clustering signals in EMC crystals. The energy deposited in nearby TOF counters is included to improve the photon reconstruction efficiency and the photon energy resolution. At least two photon candidates are selected, the minimum energy of which is required to be 25 MeV for barrel showers ($|\cos\theta| < 0.80$) and 50 MeV for end-cap showers ($0.86 < |\cos\theta| < 0.92$). To exclude showers due to the bremsstrahlung of charged particles, the angle between the nearest charged track and the shower must be greater than 10° . EMC cluster timing requirements are applied to suppress electronic noise and energy deposits unrelated to the event.

A four-constraint kinematic fit using energy-momentum conservation is performed to the $J/\psi \rightarrow K^+K^-\pi^+\pi^-\gamma\gamma$ hypothesis. All combinations of two photons are tried and the one with the smallest χ_{4C}^2 value is retained. To further suppress the background, $\chi_{4C}^2 < 200$ is required.

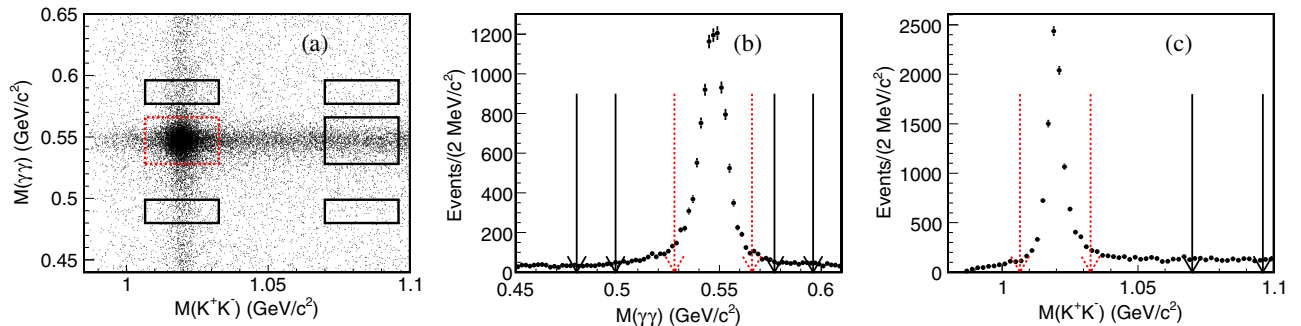


FIG. 1 (color online). (a) Scatter plot of $M(\gamma\gamma)$ versus $M(K^+K^-)$. The boxes with the dotted and solid lines show the η and ϕ signal and sideband regions, respectively. (b) The $\gamma\gamma$ invariant mass spectrum for events with the K^+K^- invariant mass in the ϕ signal region. (c) The K^+K^- invariant mass spectrum for events with the $\gamma\gamma$ invariant mass in the η signal region. In panels (b) and (c), the dotted arrows show the signal regions and the solid lines show the sideband regions, which are described in the text.

After the above selection process, a scatter plot of the invariant mass of the $\gamma\gamma$ system [$M(\gamma\gamma)$] versus the invariant mass of the K^+K^- system [$M(K^+K^-)$] in data is shown in Fig. 1(a), where the events concentrated in the region indicated by the dotted-line box correspond to the $J/\psi \rightarrow \eta\phi\pi^+\pi^-$ signal. The ϕ and η signal regions are defined as $|M(K^+K^-) - M_\phi| < 0.013 \text{ GeV}/c^2$ and $|M(\gamma\gamma) - M_\eta| < 0.019 \text{ GeV}/c^2$, where M_ϕ and M_η are world average values of the ϕ and η masses, respectively. Figures 1(b) and 1(c) show the $\gamma\gamma$ and K^+K^- invariant mass distributions for events with a K^+K^- invariant mass within the ϕ signal region and a $\gamma\gamma$ invariant mass within the η signal region, respectively. Both η and ϕ signals are clearly seen with very low background levels.

IV. MEASUREMENT OF $J/\psi \rightarrow \eta Y(2175)$ WITH $Y(2175) \rightarrow \phi f_0(980)$ AND $f_0(980) \rightarrow \pi^+\pi^-$

With the above requirements on the η and ϕ candidate masses, the $\pi^+\pi^-$ invariant mass distribution is shown in Fig. 2(a). A clear $f_0(980)$ signal is visible. The non- ϕ and/or non- η backgrounds are estimated with the events in the η - ϕ sideband regions, shown as the shaded histogram in Fig. 2(a). The η sideband is defined by $0.480 \text{ GeV}/c^2 < M(\gamma\gamma) < 0.499 \text{ GeV}/c^2$ or $0.577 \text{ GeV}/c^2 < M(\gamma\gamma) < 0.596 \text{ GeV}/c^2$, and the ϕ sideband is defined by $1.070 \text{ GeV}/c^2 < M(K^+K^-) < 1.096 \text{ GeV}/c^2$. Using a mass requirement of $0.90 \text{ GeV}/c^2 < M(\pi^+\pi^-) < 1.05 \text{ GeV}/c^2$

to select the $f_0(980)$ signal, the invariant mass distribution of $\phi f_0(980)$ is shown in Fig. 2(d), where a broad structure around $2.2 \text{ GeV}/c^2$ is evident. Figure 2(c) shows a two-dimensional histogram of $M(\phi\pi^+\pi^-)$ versus $M(\pi^+\pi^-)$. A cluster of events populating the $Y(2175)$ and $f_0(980)$ signal regions is observed, which corresponds to the decay of $Y(2175) \rightarrow \phi f_0(980)$ with $f_0(980) \rightarrow \pi^+\pi^-$.

Since the contribution from non- η background events in the $f_0(980)$ mass region is small and can be neglected, the two-dimensional ϕ - $f_0(980)$ sidebands are used to estimate the background events in this analysis. With the η mass requirement applied, the non- ϕ and/or non- $f_0(980)$ events are estimated by the weighted sums of horizontal and vertical sidebands, with the entries in the diagonal sidebands subtracted to compensate for the double counting of background components. The definition of the two-dimensional sidebands is illustrated in Fig. 2(b). The weighting factors for the events in the horizontal, vertical, and diagonal sidebands are measured to be 0, and 0.66, -0.085 , respectively, which are determined from the results of a two-dimensional fit to the mass spectrum of $M(K^+K^-)$ versus $M(\pi^+\pi^-)$. No signal of $f_0(980)$ is evident in non- ϕ processes as shown in the scatter plot of $M(\pi^+\pi^-)$ versus $M(K^+K^-)$. Hence, the weighting factor for the events in the horizontal sideband is zero, and the non- ϕ events in the horizontal sideband are not used in the background estimation. The two-dimensional probability density functions (PDFs) for $J/\psi \rightarrow \eta\phi f_0(980)$, ϕ but non- $f_0(980)$,

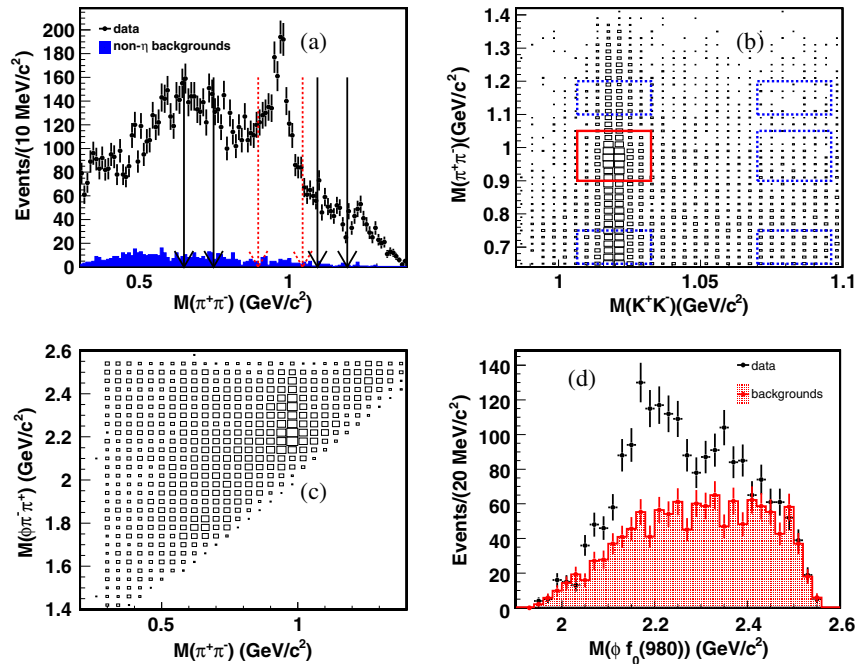


FIG. 2 (color online). (a) The $\pi^+\pi^-$ invariant mass spectrum. The shaded histogram shows the non- η background estimated with the η sideband region; the dotted and solid arrows denote the $f_0(980)$ signal and sideband regions, respectively. (b) The scatter plot of $M(\pi^+\pi^-)$ versus $M(K^+K^-)$. The solid box shows the signal region, and the dotted boxes show the sideband regions of ϕ and f_0 . (c) The scatter plot of $M(\phi\pi^+\pi^-)$ versus $M(\pi^+\pi^-)$. (d) The $\phi\pi^+\pi^-$ invariant mass distribution after imposing the $f_0(980)$ signal mass window requirement. The shaded histogram shows the background distribution estimated with the sideband method described in the text.

non- ϕ and non- $f_0(980)$ processes are constructed by the product of one-dimensional functions, where the resonant peaks are parametrized by Breit-Wigner functions (for ϕ) and a shape taken from simulation [for $f_0(980)$], and the nonresonant parts are described by polynomials with coefficients left free in the fit. To account for the difference of the background shape between the signal region and sidebands due to the varying phase space, the obtained background mass distribution is multiplied by a correction curve determined from a MC sample of 1×10^6 events of the phase space processes $J/\psi \rightarrow \eta\phi\pi^+\pi^-$. The estimated $K^+K^-\pi^+\pi^-$ invariant mass distribution for the total non- ϕ or non- $f_0(980)$ components is shown by the shaded histogram in Fig. 2(d). No evident $Y(2175)$ signal is observed.

To extract the yield of $Y(2175)$, an unbinned maximum likelihood fit to the $\phi f_0(980)$ invariant mass is performed. The $Y(2175)$ signal, the direct three-body decay of $J/\psi \rightarrow \eta\phi f_0(980)$, and the background from the above estimation shown as the shaded histogram in Fig. 2(b) are included in the fit. With the assumption of no interference between the $Y(2175)$ signal and the direct three-body decay of $J/\psi \rightarrow \eta\phi f_0(980)$, the PDF can be written as

$$\epsilon(m) \times (G \otimes |A(m)|^2) + A(J/\psi \rightarrow \eta\phi f_0) + \text{BKG}, \quad (1)$$

where $A(m) = \frac{P_{J \rightarrow \eta}^{l_1} P_{Y \rightarrow \phi f_0}^{l_2}}{m^2 - M_0^2 + iM_0\Gamma_0}$ is a Breit-Wigner function representing the $Y(2175)$ signal shape, taking into account the phase space factor of a two-body decay. M_0 and Γ_0 are left free in the fit. $P_{J \rightarrow \eta}$ and $P_{Y \rightarrow \phi f_0}$ denote the momentum of the η in the rest frame of the J/ψ and that of the ϕ in the rest frame of the $Y(2175)$, respectively. l_1 and l_2 , which label the relative orbital angular momenta of the η - $Y(2175)$ and ϕ - $f_0(980)$ systems, are set to be 1 and 0 in the fit, respectively. G is a Gaussian function representing the mass resolution, and the corresponding parameters are taken from a MC simulation. $\epsilon(m)$, the detection efficiency as a function of the $\phi f_0(980)$ invariant mass, is also obtained from a MC simulation. $A(J/\psi \rightarrow \eta\phi f_0)$ represents the component of the direct decay of $J/\psi \rightarrow \eta\phi f_0(980)$ with the shape derived from the phase space MC sample. Finally, BKG refers to the background component estimated from the two-dimensional weighted sideband method.

Figure 3 shows the results of the fit, where the circular dots with error bars show the distribution for the signal and the triangular dots with error bars are for the backgrounds estimated by the sidebands. The solid curve is the overall fit projection, the dotted curve the fit for the backgrounds, and the dashed curve for the sum of the direct decay of $J/\psi \rightarrow \eta\phi f_0$ and the backgrounds. The mass and width of the $Y(2175)$ are determined to be $M = 2200 \pm 6 \text{ MeV}/c^2$ and $\Gamma = 104 \pm 15 \text{ MeV}$, respectively. The fit yields 471 ± 54 $Y(2175)$ events with a statistical significance of greater than 10σ , which is determined by the change of the

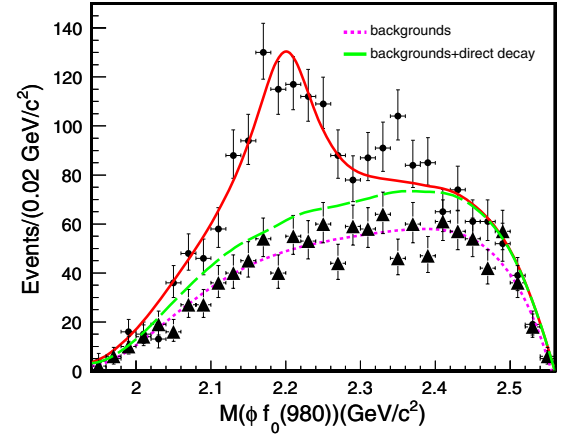


FIG. 3 (color online). Result of the fit to the $\phi f_0(980)$ invariant mass distribution described in the text. The circular dots with error bars show the distribution in the signal region; the triangular dots with error bars show the backgrounds estimated using sideband regions; the solid curve shows the overall fit projection; the dotted curve shows the fit for the backgrounds; and the dashed curve is for the sum of the direct decay of $J/\psi \rightarrow \eta\phi f_0$ and the backgrounds.

log-likelihood value and the number of degree of freedom in the fit with and without the $Y(2175)$ signal. Taking into account the detection efficiency, $(9.10 \pm 0.01)\%$, obtained from a MC simulation, the product branching fraction is

$$\mathcal{B}(J/\psi \rightarrow \eta Y(2175), \quad Y(2175) \rightarrow \phi f_0(980), \\ f_0(980) \rightarrow \pi^+\pi^-) = (1.20 \pm 0.14) \times 10^{-4}.$$

We also perform a fit to the $\phi f_0(980)$ invariant mass, allowing interference between the $Y(2175)$ and the direct decay $J/\psi \rightarrow \eta\phi f_0(980)$. An ambiguity in the phase angle

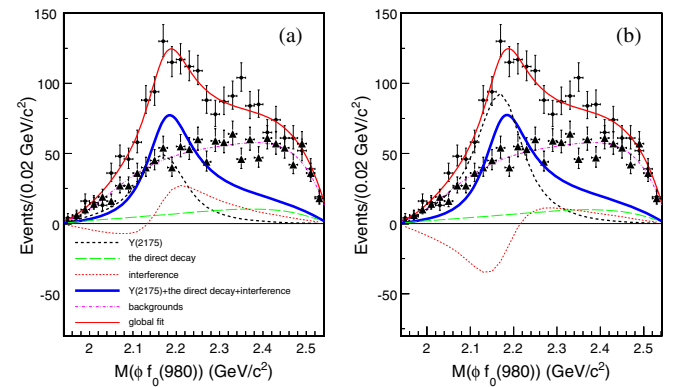


FIG. 4 (color online). The fit projections to the $\phi f_0(980)$ invariant mass distribution showing the (a) constructive and (b) destructive solutions. The short-dashed line denotes the signal distribution; the dot-dashed curve shows the fit to the backgrounds estimated by the sidebands; the long-dashed line denotes the direct decay of $J/\psi \rightarrow \eta\phi f_0$; and the dotted line denotes the interference component.

TABLE I. Two solutions of the fit to $M(\phi f_0(980))$, taking interference with the direct decay $\eta\phi f_0$ into account. Errors are statistical only.

Parameters	Constructive	Destructive
M (MeV/ c^2)	2171 ± 10	2170 ± 9
Γ (MeV)	128 ± 26	126 ± 25
Signal yields	400 ± 167	744 ± 40
relative angle Φ (rad)	-0.51 ± 0.78	0.60 ± 0.64

occurs when a resonance interferes with a varying continuum [42]. Thus, two solutions with different relative phase angles, corresponding to constructive and destructive interferences, are found. The final fit and the individual contributions of each of the components are shown in Figs. 4(a) and 4(b) for constructive and destructive interference, respectively. The mass, width, and yields of the $Y(2175)$ signal, as well as the relative phase angle, are shown in Table I. The statistical significance of the interference is 2.5σ , which is determined from the differences of the likelihood values and the degrees of freedom between the fits with and without interference. In this analysis, the fit results without considering interference are taken as the nominal values.

V. MEASUREMENT OF $J/\psi \rightarrow \phi f_1(1285)$ AND $\phi\eta(1405)$

The $\eta\pi^+\pi^-$ mass spectrum recoiling against the ϕ is shown in Fig. 5. Besides the significant and well-known $f_1(1285)$ signal, a small structure around 1.4 GeV/ c^2 , which is assumed to be the $\eta(1405)$, is evident over a large

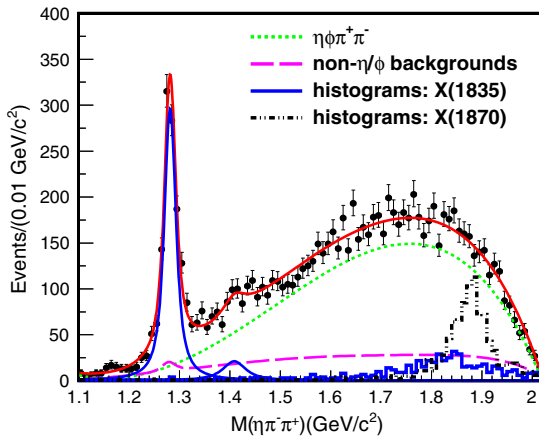


FIG. 5 (color online). Fit to the $\eta\pi^+\pi^-$ invariant mass spectrum. The solid lines show the total fit and the $f_1(1285)$ and $\eta(1405)$ components; the dashed line denotes the non- η and non- ϕ background estimated using the η - ϕ sidebands; the dotted curve represents the $J/\psi \rightarrow \eta\phi\pi^+\pi^-$ component; the solid histogram indicates the shape of the $X(1835)$ (with arbitrary normalization); and the dash-dotted histogram shows the predicted shape of the $X(1870)$ signal (with arbitrary normalization).

nonresonant background. A fit to the $\eta\pi^+\pi^-$ invariant mass is performed with a PDF that includes contributions from the $f_1(1285)$ and $\eta(1405)$ signals, the decay $J/\psi \rightarrow \eta\phi\pi^+\pi^-$ [including the process $J/\psi \rightarrow \eta\phi f_0(980)$], and backgrounds from non- η and non- ϕ processes. In the fit, the $f_1(1285)$ and $\eta(1405)$ signal shapes are described by Breit-Wigner functions convoluted with Gaussian functions for their mass resolutions. The mass and width of the $f_1(1285)$ signal are left free in the fit, while those of the $\eta(1405)$ signal are fixed to the values in the PDG [1]. The parameters of the Gaussian functions for the mass resolutions are fixed to their MC values. The shape of the $J/\psi \rightarrow \eta\phi\pi^+\pi^-$ decay is represented by a third-order Chebychev polynomial function, and the corresponding parameters are allowed to vary. The non- η and non- ϕ background is estimated with the events in the η - ϕ sideband regions, as shown by the dashed lines in Fig. 5, and is fixed in the fit.

The fit, shown in Fig. 5, yields 1154 ± 56 $f_1(1285)$ signal events, with a mass of 1281.7 ± 0.6 MeV/ c^2 and a width of 21.0 ± 1.7 MeV. The mass and width are in good agreement with world average values [1]. Using a detection efficiency of $(22.14 \pm 0.09)\%$, obtained from a MC simulation, the product branching fraction is measured to be

$$\begin{aligned} \mathcal{B}(J/\psi \rightarrow \phi f_1(1285)), \\ f_1(1285) \rightarrow \eta\pi^+\pi^-) = (1.20 \pm 0.06) \times 10^{-4}, \end{aligned}$$

where the error is statistical only.

For the $\eta(1405)$ signal, the fit yields 172 ± 50 events with a statistical significance of 3.6σ , evaluated from the difference of the likelihood values between the fits with and without the $\eta(1405)$ included. The product branching fraction is $\mathcal{B}(J/\psi \rightarrow \phi\eta(1405), \eta(1405) \rightarrow \eta\pi^+\pi^-) = (2.01 \pm 0.58) \times 10^{-5}$, where the error is statistical only. To determine the upper limit on the $\eta(1405)$ production rate, a series of similar fits with given numbers of $\eta(1405)$ events are performed, and the likelihood values of the fits as a function of the number of $\eta(1405)$ events are taken as a normalized probability function. The upper limit on the number of signal events at the 90% C.L., $N^{U.L.}$, is defined as the value that contains 90% of the integral of the normalized probability function. The fit-related uncertainties on $N^{U.L.}$ are estimated by using different sideband regions for the effect of the non- η and non- ϕ background, different orders of Chebychev polynomials for the shape of the $J/\psi \rightarrow \eta\phi\pi^+\pi^-$, and changing the mass and width values of the $\eta(1405)$ within one standard deviation from the central values for the signal shape. Finally, after taking into account fit-related uncertainties, we obtain $N^{U.L.} = 345$. This upper limit and the detection efficiency of $(19.75 \pm 0.12)\%$, estimated from a MC simulation, are used to evaluate the upper limit on the branching fraction:

$$\mathcal{B}(J/\psi \rightarrow \phi\eta(1405), \eta(1405) \rightarrow \eta\pi^+\pi^-)$$

$$\begin{aligned} & \frac{N^{U.L.}}{\epsilon \times N_{J/\psi} \times \mathcal{B}(\eta \rightarrow \gamma\gamma) \times \mathcal{B}(\phi \rightarrow K^+K^-) \times (1 - \sigma_{\text{sys}})} \\ & = 4.45 \times 10^{-5}, \end{aligned} \quad (2)$$

where σ_{sys} is the systematic error to be discussed in detail below. Since the background uncertainty is taken into account in the calculation of $N^{U.L.}$ by choosing the maximum event yield from the variations of the background functions, the systematic uncertainty from this source is excluded here. The final results on the upper limit of the branching fraction are shown in Table III.

In the $\eta\pi^+\pi^-$ mass spectrum shown in Fig. 5, we do not observe obvious structures around $1.84 \text{ GeV}/c^2$ or at $1.87 \text{ GeV}/c^2$. Using the same approach as was used for the $\eta(1405)$, we set 90% C.L. upper limits for the $X(1835)$ and $X(1870)$ production rates, where the signal shape of the $X(1835)$ or $X(1870)$ is described by a Breit-Wigner function convoluted with a Gaussian function for the mass resolution, and the background is modeled by a third-order Chebychev polynomial. The resonant parameters of the $X(1835)$ and $X(1870)$ are fixed to the values of previous BESIII measurements [22,23]. The results are summarized in Tables II and III.

TABLE II. Measurements of the number of events, statistical significances, and efficiencies.

Resonance	N_{obs}	Significance	Efficiency(%)
$Y(2175)$	471 ± 54	$> 10\sigma$	9.10 ± 0.01
$f_1(1285)$	1154 ± 56	\dots	22.14 ± 0.09
$\eta(1405)$	$172 \pm 50 (< 345)$	3.6σ	19.75 ± 0.12
$X(1835)$	$394 \pm 360 (< 1522)$	1.1σ	13.85 ± 0.14
$X(1870)$	$25 \pm 73 (< 330)$	0.8σ	13.73 ± 0.14

TABLE III. Measurements of the branching fractions for the decay modes. Upper limits are given at the 90% C.L.

Decay mode	Branching fraction \mathcal{B}
$J/\psi \rightarrow \eta Y(2175),$ $Y(2175) \rightarrow \phi f_0(980),$ $f_0(980) \rightarrow \pi^+\pi^-$	$(1.20 \pm 0.14 \pm 0.37) \times 10^{-4}$
$J/\psi \rightarrow \phi f_1(1285),$ $f_1(1285) \rightarrow \eta\pi^+\pi^-$	$(1.20 \pm 0.06 \pm 0.14) \times 10^{-4}$
$J/\psi \rightarrow \phi\eta(1405),$ $\eta(1405) \rightarrow \eta\pi^+\pi^-$	$(2.01 \pm 0.58 \pm 0.82)$ $(< 4.45) \times 10^{-5}$
$J/\psi \rightarrow \phi X(1835),$ $X(1835) \rightarrow \eta\pi^+\pi^-$	$< 2.80 \times 10^{-4}$
$J/\psi \rightarrow \phi X(1870),$ $X(1870) \rightarrow \eta\pi^+\pi^-$	$< 6.13 \times 10^{-5}$

VI. SYSTEMATIC ERRORS

The sources of systematic error include the efficiency difference between data and MC simulation for the track reconstruction, the PID, the photon detection, and the kinematic fit; the fitting procedure; the ambiguity in the interference; and the number of J/ψ events. Their effects on the measurement of the resonance parameters and the branching fractions are discussed in detail below.

- MDC tracking efficiency*—The tracking efficiency has been investigated using the almost background-free control samples of $J/\psi \rightarrow \pi^+\pi^-p\bar{p}$ and $J/\psi \rightarrow K_S^0 K\pi$ [43]. The difference in tracking efficiency between data and MC is found to be 2% per charged kaon and pion. Therefore, 8% is taken as the total systematic error for the detection efficiency of four charged tracks.
- PID efficiency*—To evaluate the PID efficiency uncertainty, we have studied the kaon and pion PID efficiencies using the control samples of $J/\psi \rightarrow K^{*\pm}K^\mp$ and $J/\psi \rightarrow \rho\pi$ [43], respectively. The difference in PID efficiency between data and MC is 1% per kaon and pion. Hence, 4% is taken as the total systematic error from the PID efficiency.
- Photon detection efficiency*—The photon detection efficiency has been studied using a control sample of $J/\psi \rightarrow \rho\pi$ [43]. The difference between data and MC is found to be 1% per photon. Therefore, 2% is taken as the total systematic error for the efficiency of the detection of the two photons.
- Kinematic fit*—To estimate the uncertainty associated with the kinematic fit, a control sample of $J/\psi \rightarrow \phi\eta'(\eta' \rightarrow \eta\pi^+\pi^-)$, which has exactly the same final state as the signal, is first selected without a kinematic fit. The kinematic fit efficiency is then evaluated from the ratio of the η' yields with and without the kinematic fit requirement, where the η' yield is extracted from the fit to the η' signal in the $\eta\pi^+\pi^-$ invariant mass. The difference of the kinematic fit efficiency between data and MC, 0.4%, is taken as the systematic error for the kinematic fit.
- Uncertainties of $\mathcal{B}(\eta \rightarrow \gamma\gamma)$ and $\mathcal{B}(\phi \rightarrow K^+K^-)$* —The branching fractions of $\eta \rightarrow \gamma\gamma$ and $\phi \rightarrow K^+K^-$ are taken from the PDG [1]. The uncertainties of these branching fractions, 0.5% and 1.0%, are taken as the systematic errors.
- Uncertainty of the number of J/ψ events*—The total number of J/ψ events is determined from an analysis of inclusive J/ψ hadronic decays, and the uncertainty of the number of J/ψ events, 1.2% [44], is taken as the systematic error from the number of J/ψ events.
- Background uncertainty*—In the measurement of the resonance parameters and branching fractions of the $Y(2175)$, a fit is performed to the $\phi f_0(980)$ invariant mass spectrum. In the fit, the shape and amplitude of the background from the non- ϕ and non- $f_0(980)$ are

fixed to the estimation from the ϕ - $f_0(980)$ sideband regions. To estimate its impact on the final results, we use different ϕ - $f_0(980)$ sideband regions to estimate the background, and follow the same fit procedure. The maximum changes on both the $Y(2175)$ resonance parameters and its signal yield are taken as the systematic errors. The uncertainty due to the background on the mass and width of the $Y(2175)$ are $\pm 4.0 \text{ MeV}/c^2$ and $\pm 14.0 \text{ MeV}$, respectively.

For the branching fraction of $J/\psi \rightarrow \phi f_1(1285)/\eta(1405)$ with $f_1(1285)/\eta(1405) \rightarrow \eta\pi^+\pi^-$, the non- η and non- ϕ backgrounds are estimated with the events in the η - ϕ sideband regions. Analogous to the evaluation of the $Y(2175)$ errors, we define different sideband regions to estimate the backgrounds and follow the same fit procedure. The largest changes are taken as the uncertainty from the background for these measurements. Compared to the number of $f_1(1285)$ events, the fluctuation of background shape under the $\eta(1405)$ peak has a large impact on the signal yields in the fit due to the limited statistics.

- (h) *Impact from possible extra resonances*—In the invariant mass spectrum of $\phi f_0(980)$, a small structure around $2.35 \text{ GeV}/c^2$ is found (Fig. 3). To evaluate its impact on the $Y(2175)$ measurement, we perform a fit with an additional signal around $2.35 \text{ GeV}/c^2$, which is described with a Breit-Wigner function convoluted with a Gaussian function for the mass resolution. The fit results show that the significance of the structure around $2.35 \text{ GeV}/c^2$ is only 3.8σ . It is therefore not considered in the nominal final results. However, the impact on the $Y(2175)$ measurement is taken as the systematic error. The uncertainty due to the possible extra resonance on the mass and width of the $Y(2175)$ is $\pm 3.0 \text{ MeV}/c^2$ and $\pm 5.0 \text{ MeV}$, respectively.

In the measurement of the branching fraction of $J/\psi \rightarrow \phi f_1(1285)$ with $f_1(1285) \rightarrow \eta\pi^+\pi^-$, we perform

a fit without the $\eta(1405)$ signal. The difference of results with or without the $\eta(1405)$ signal included in the fit is taken as the systematic error on the $f_1(1285)$ measurement from the impact of the $\eta(1405)$.

- (i) *Parametrization of the $f_0(980)$* —The systematic error from the $f_0(980)$ shape is estimated by comparing the detection efficiencies from the signal MC samples simulated with different parametrizations of the $f_0(980)$. We use the resonant parameters of the $f_0(980)$ from Ref. [45], instead of the nominal values from the measurements of BESII [41] mentioned in Sec. II, to describe the $f_0(980)$ shape. This leads to a difference in the detection efficiency of 7.6%, and is taken as the systematic uncertainty on the $Y(2175)$ branching fraction measurement from the $f_0(980)$ parametrization.
- (j) *Uncertainty from fixed mass and width values on the branching ratio of $J/\psi \rightarrow \phi\eta(1405)$ with $\eta(1405) \rightarrow \eta\pi^+\pi^-$* —The mass and width of the $\eta(1405)$ are fixed to their PDG values in the fit to the $\eta(1405)$ signal. We change the mass and width values by one standard deviation from their central values in the fitting procedure. The maximum change on the branching fraction is determined to be 7.0% when the mass and width values are fixed at one negative standard deviation from the central values.
- (k) *Uncertainty from parameter sets in the generation of $J/\psi \rightarrow \phi f_1(1285)$* —The parameters used in the generation of the signal MC sample of $J/\psi \rightarrow \phi f_1(1285)$ are taken from the angular distribution of the ϕ in the rest frame of the J/ψ found in real data. The impact of the uncertainty of these parameters on the efficiency, 3.2%, is taken as a source of systematic error on the branching fraction.

In Table IV, a summary of all contributions to the systematic errors on the branching fraction measurements is shown. In each case, the total systematic uncertainty is

TABLE IV. Summary of systematic errors (in %) for the branching fraction measurements. The fourth column shows the sources of systematic errors on the branching fraction of $J/\psi \rightarrow \phi\eta(1405)$ with $\eta(1405) \rightarrow \eta\pi^+\pi^-$, while the fifth column shows those on the upper limits of the branching fractions of $J/\psi \rightarrow \phi\eta(1405)$, $\phi X(1835)$, $\phi X(1870)$ with $\eta(1405)/X(1835)/X(1870) \rightarrow \eta\pi^+\pi^-$.

Sources	$Y(2175)$	$f_1(1285)$	$\eta(1405)$	$\eta(1405)/X(1835)/X(1870)$
MDC tracking			8.0	
Photon detection			2.0	
PID			4.0	
Kinematic fit			0.4	
$\mathcal{B}(\eta \rightarrow \gamma\gamma)$			0.5	
$\mathcal{B}(\phi \rightarrow K^+K^-)$			1.0	
Number of J/ψ events			1.2	
$f_0(980)$ selection	7.6
Background uncertainty	19.1	4.1	39.3	...
The fixed M/Γ of $\eta(1405)$	7.0	...
Parameters of $\phi f_1(1285)$ generation	...	3.2
Extra resonance	21.4	4.0
Total	31.1	11.4	41.0	9.4

TABLE V. Comparison of $Y(2175)$ parameters as measured by different experiments.

Collaboration	Process	M (MeV/ c^2)	Γ (MeV)
BABAR [2]	$e^+e^- \rightarrow \phi f_0$ (ISR)	$2175 \pm 10 \pm 15$	$58 \pm 16 \pm 20$
BESII [3]	$J/\psi \rightarrow \eta \phi f_0(980)$	$2186 \pm 10 \pm 6$	$65 \pm 23 \pm 17$
BELLE [4]	$e^+e^- \rightarrow \phi f_0$ (ISR)	$2079 \pm 13_{-28}^{+79}$	$192 \pm 23_{-61}^{+25}$
BABAR (updated) [5]	$e^+e^- \rightarrow \phi f_0$ (ISR)	$2172 \pm 10 \pm 8$	$96 \pm 19 \pm 12$
BESIII	$J/\psi \rightarrow \eta \phi f_0(980)$	$2200 \pm 6 \pm 5$	$104 \pm 15 \pm 15$

obtained by adding the individual contributions in quadrature. For the uncertainties on the $Y(2175)$ resonant parameters, we find that the dominant systematic uncertainties are from the background shape and a possible additional resonance around $2.35 \text{ GeV}/c^2$. Adding the various systematic uncertainties in quadrature, the total systematic errors on the mass and width of the $Y(2175)$ are $\pm 5.0 \text{ MeV}/c^2$ and $\pm 14.8 \text{ MeV}$, respectively.

VII. SUMMARY

In summary, we present an analysis of $J/\psi \rightarrow \eta \phi \pi^+ \pi^-$ based on $(225.3 \pm 2.8) \times 10^6$ J/ψ events collected with the BESIII detector. The $Y(2175)$ resonance is observed in the invariant mass spectrum of $\phi f_0(980)$ with a statistical significance of greater than 10σ . The mass and width of the $Y(2175)$ are measured and are in good agreement with previous experimental results (Table V). Neglecting the effects of interference with the direct decay $J/\psi \rightarrow \eta \phi f_0(980)$, the product branching fraction is measured to be $\mathcal{B}(J/\psi \rightarrow \eta Y(2175), Y(2175) \rightarrow \phi f_0(980), f_0(980) \rightarrow \pi^+ \pi^-) = (1.20 \pm 0.14 \pm 0.37) \times 10^{-4}$. We also perform a fit taking the interference between the $Y(2175)$ and the direct decay. The corresponding results are shown in Table I.

In addition, we investigate the $\eta \pi^+ \pi^-$ mass spectrum recoiling against the ϕ in the J/ψ decay. A structure around $1.28 \text{ GeV}/c^2$ is clearly seen, and the fit results are in good agreement with the world average values of the $f_1(1285)$ parameters. The product branching fraction of $J/\psi \rightarrow \phi f_1(1285)$ with $f_1(1285) \rightarrow \eta \pi^+ \pi^-$ is measured to be $\mathcal{B}(J/\psi \rightarrow \phi f_1(1285) \rightarrow \phi \eta \pi^+ \pi^-) = (1.20 \pm 0.06 \pm 0.14) \times 10^{-4}$. A structure around $1.4 \text{ GeV}/c^2$ seems to be present in the $\eta \pi^+ \pi^-$ mass spectrum. Assuming it to be the $\eta(1405)$, the product branching fraction is calculated to be $\mathcal{B}(J/\psi \rightarrow \phi \eta(1405) \rightarrow \phi \eta \pi^+ \pi^-) = (2.01 \pm 0.58 \pm 0.82) \times 10^{-5}$. We also present a 90% C.L. upper limit on the branching fraction $\mathcal{B}(J/\psi \rightarrow \phi \eta(1405), \eta(1405) \rightarrow \eta \pi^+ \pi^-) < 4.45 \times 10^{-5}$. In a previous experiment, the $\eta(1405)/\eta(1440)$ is observed in both $\eta \pi \pi$ and $K \bar{K} \pi$ invariant mass spectra recoiling against the γ and ω in J/ψ decays. However, no significant structure around $1.4 \text{ GeV}/c^2$ is observed in the $\pi^+ \pi^- \eta$ mass spectrum recoiling against the

ϕ in this analysis, which may imply that u and d quarks account for more of the quark content in the $\eta(1405)$ than the s quark. We also perform searches for the $X(1835)$ and $X(1870)$ in the vicinity of $1.8 \text{ GeV}/c^2$ in the $\eta \pi^+ \pi^-$ mass spectrum, and observe no evident structures. The corresponding upper limits at 90% C.L. of branching fraction are measured. All of these measurements provide information in understanding the nature of the $X(1835)$ and $X(1870)$.

ACKNOWLEDGMENTS

The BESIII Collaboration thanks the staff of BEPCII and the IHEP computing center for their strong support. This work is supported in part by National Key Basic Research Program of China under Contract No. 2015CB856700; Joint Funds of the National Natural Science Foundation of China under Contracts No. 11079008, No. 11179007, No. U1232201, and No. U1332201; National Natural Science Foundation of China (NSFC) under Contracts No. 10935007, No. 11121092, No. 11125525, No. 11235011, No. 11322544, No. 11335008, No. 11175189, and No. 11375204; the Chinese Academy of Sciences (CAS) Large-Scale Scientific Facility Program; CAS under Contracts No. KJCX2-YW-N29 and No. KJCX2-YW-N45; the 100 Talents Program of CAS; INPAC and the Shanghai Key Laboratory for Particle Physics and Cosmology; the German Research Foundation DFG under Contract No. Collaborative Research Center CRC-1044; Istituto Nazionale di Fisica Nucleare, Italy; Ministry of Development of Turkey under Contract No. DPT2006K-120470; Russian Foundation for Basic Research under Contract No. 14-07-91152; U.S. Department of Energy under Contracts No. DE-FG02-04ER41291, No. DE-FG02-05ER41374, No. DE-FG02-94ER40823, and No. DESC0010118; the U.S. National Science Foundation; the University of Groningen (RuG) and the Helmholtzzentrum fuer Schwerionenforschung GmbH (GSI), Darmstadt; and the WCU Program of the National Research Foundation of Korea under Contract No. R32-2008-000-10155-0.

- [1] K. A. Olive *et al.* (Particle Data Group), *Chin. Phys. C* **38**, 090001 (2014).
- [2] B. Aubert *et al.* (BABAR Collaboration), *Phys. Rev. D* **74**, 091103(R) (2006).
- [3] M. Ablikim *et al.* (BES Collaboration), *Phys. Rev. Lett.* **100**, 102003 (2008).
- [4] C. P. Shen *et al.* (BELLE Collaboration), *Phys. Rev. D* **80**, 031101(R)(2009).
- [5] J. P. Lees *et al.* (BABAR Collaboration), *Phys. Rev. D* **86**, 012008 (2012).
- [6] B. Aubert *et al.*, *Phys. Rev. Lett.* **95**, 142001 (2005).
- [7] C. Z. Yuan *et al.* (BELLE Collaboration), *Phys. Rev. Lett.* **99**, 182004 (2007).
- [8] G. J. Ding and M. L. Yan, *Phys. Lett. B* **650**, 390 (2007).
- [9] G. J. Ding and M. L. Yan, *Phys. Lett. B* **657**, 49 (2007).
- [10] Z. G. Wang, *Nucl. Phys. A* **791**, 106 (2007).
- [11] E. Klempt and A. Zaitsev, *Phys. Rep.* **454**, 1 (2007).
- [12] C. F. Qiao, *Phys. Lett. B* **639**, 263 (2006).
- [13] A. Martinez Torres, K. P. Khemchandani, L. S. Geng, M. Napsuciale, and E. Oset, *Phys. Rev. D* **78**, 074031 (2008).
- [14] S. L. Zhu, *Int. J. Mod. Phys. E* **17**, 283 (2008).
- [15] T. Barnes, N. Black, and P. R. Page, *Phys. Rev. D* **68**, 054014 (2003).
- [16] W.-M. Yao *et al.*, *J. Phys. G* **33**, 1 (2006).
- [17] J. J. Manak *et al.*, *Phys. Rev. D* **62**, 012003 (2000).
- [18] D. L. Scharre *et al.*, *Phys. Lett.* **97B**, 329 (1980).
- [19] H. J. Behrend *et al.* (CELLO Collaboration), *Z. Phys. C* **42**, 367 (1989).
- [20] I. Vodopianov *et al.* (L3 Collaboration), *Acta Phys. Pol. B* **31**, 2453 (2000).
- [21] M. Ablikim *et al.* (BES Collaboration), *Phys. Rev. Lett.* **95**, 262001 (2005).
- [22] M. Ablikim *et al.* (BESIII Collaboration), *Phys. Rev. Lett.* **106**, 072002 (2011).
- [23] M. Ablikim *et al.* (BESIII Collaboration), *Phys. Rev. Lett.* **107**, 182001 (2011).
- [24] C. S. Gao and S. L. Zhu, *Commun. Theor. Phys.* **42**, 844 (2004).
- [25] G. J. Ding and M. L. Yan, *Phys. Rev. C* **72**, 015208 (2005).
- [26] G. Hao, C. F. Qiao, and A. L. Zhang, *Phys. Lett. B* **642**, 53 (2006).
- [27] B. A. Li, *Phys. Rev. D* **74**, 034019 (2006).
- [28] N. Kochelev and D. P. Min, *Phys. Lett. B* **633**, 283 (2006).
- [29] B. Kerbikov, A. Stavinsky, and V. Fedotov, *Phys. Rev. C* **69**, 055205 (2004).
- [30] D. V. Bugg, *Phys. Lett. B* **598**, 8 (2004).
- [31] B. S. Zou and H. C. Chiang, *Phys. Rev. D* **69**, 034004 (2004).
- [32] M. Ablikim *et al.* (BESIII Collaboration), *Nucl. Instrum. Methods Phys. Res., Sect. A* **614**, 345 (2010).
- [33] Z. Y. Deng *et al.*, *High Energy Phys. Nucl. Phys.* **30**, 371 (2006).
- [34] S. Jadach, B. F. L. Ward, and Z. Was, *Comput. Phys. Commun.* **130**, 260 (2000).
- [35] S. Jadach, B. F. L. Ward, and Z. Was, *Phys. Rev. D* **63**, 113009 (2001).
- [36] K. T. Chao *et al.*, *Mod. Phys. Lett. A* **24**, S1 (2009).
- [37] R. G. Ping, *Chin. Phys. C* **32**, 599 (2008).
- [38] D. J. Lange, *Nucl. Instrum. Methods Phys. Res., Sect. A* **462**, 152 (2001).
- [39] J. C. Chen, G. S. Huang, X. R. Qi, D. H. Zhang, and Y. S. Zhu, *Phys. Rev. D* **62**, 034003 (2000).
- [40] S. M. Flatté, *Phys. Lett.* **63B**, 224 (1976).
- [41] M. Ablikim *et al.* (BES Collaboration), *Phys. Lett. B* **607**, 243 (2005).
- [42] A. D. Bukin, On the ambiguity of the interfering resonances parameters determination, [arXiv:0710.5627](https://arxiv.org/abs/0710.5627).
- [43] M. Ablikim *et al.* (BESIII Collaboration), *Phys. Rev. D* **83**, 112005 (2011).
- [44] M. Ablikim *et al.* (BESIII Collaboration), *Chin. Phys. C* **36**, 915 (2012).
- [45] B. S. Zou and D. V. Bugg, *Phys. Rev. D* **48**, R3948 (1993).